Design and Development of an Active Magnetic Actuator for Attitude Control System of Nanosatellites

Conference Paper · December 2017

CITATIONS
0

READS
685

4 authors, including:

Simone Battistini
Sheffield Hallam University
44 PUBLICATIONS **182** CITATIONS
SEE PROFILE

Chantal Cappelletti
University of Nottingham
57 PUBLICATIONS **154** CITATIONS
SEE PROFILE

Renato A. Borges
University of Brasília
72 PUBLICATIONS **380** CITATIONS
SEE PROFILE

DESIGN AND DEVELOPMENT OF AN ACTIVE MAGNETIC ACTUATOR FOR ATTITUDE CONTROL SYSTEM OF NANOSATELLITES

Igor Seiiti Kinoshita Ishioka[*], Simone Battistini[†], Chantal Cappelletti[‡], and Renato Alves Borges[§]

This work, conducted in the Laboratory of Aerospace Science and Innovation (LAICA) at University of Brasília (UnB), reports the design and development of a triaxial active magnetic actuator for the Attitude Determination and Control System (ADCS) of nanosatellites. The ADCS is necessary for the conduction of space missions, which require stabilization and pointing capabilities. This category of small satellites is characterized by the mass, which stands in the range 1-10kg under NASA's classification. As one of the requisites, the actuator shall be modular and compatible with the CubeSat dimensional standard. The testing campaign, which is part of the work, will be conducted through the ADCS testbed available and developed in the same laboratory. The testbed is equipped with a Helmholtz cage for simulation of Earth's magnetic field in orbital conditions, allowing the verification of the behavior of the triaxial system and therefore its preliminary characterization.

INTRODUCTION

In order to contribute to the research on satellite Attitude Determination and Control Systems (ADCS) in the Laboratory of Aerospace Science and Innovation (LAICA) of University of Brasília (UnB), there is the demand for the design and development of the magnetic actuator for nanosatellites. The actuator to be developed may in later stages be used for the development and testing of control laws, and also for conducting optimizations of the testbed of the laboratory.

Nanosatellites are characterized by their mass ranging from 1 to 10kg according to NASA's classification.[1] The use of nanosatellites is directly related to their reduced cost, and the small size of the subsystems is possible thanks to the technological advancements. Mass and size may impose significant limitations on certain types of mission, such as those for telecommunication purposes and involving large payloads, but are convenient for others which have, for example, educational and systems testing objectives.

As part of the research carried out in the laboratory, it coordinated the SERPENS nanosatellite project, a 3U CubeSat funded by the Brazilian Space Agency (AEB) and developed by a university consortium with AEB. The main objective of the mission was to promote the training of students

[*]Faculdade do Gama, Universidade de Brasília, Gama-DF, Brazil, igorseiiti@gmail.com
[†]Faculdade do Gama, Universidade de Brasília, Gama-DF, Brazil, simone.battistini@aerospace.unb.br
[‡]Faculdade do Gama, Universidade de Brasília, Gama-DF, Brazil, chantal@aerospace.unb.br
[§]Faculdade de Tecnologia, Universidade de Brasília, Brasília-DF, Brazil, raborges@aerospace.unb.br

and engineers in space technology, the functionally being a proof of concept of the Brazilian data collection system.[2]

With regard to the spacecraft attitude active actuators, the reaction wheels, magnetic actuators, cold gas thrusters, and others are generally used.[3,4] Due to the large compaction and variety, the reaction wheels can be used in both large and small satellites. Cold gas thrusters are a more complex system for use in nanosatellites due to the volume and mass added by the system.

The most common magnetic actuators are composed of electromagnetic coils, but there are also other more complex such as the electrodynamic tether, they function through the interaction with the geomagnetic field. Because of this fact, they are used in Low Earth Orbit (LEO) missions where the magnitude of the geomagnetic field is greater.

As advantages of using electromagnetic coils as attitude actuators, can be pointed the relatively small mass of these systems, the absence of moving parts, no need for propellants and low cost. Much of the mass associated to the coils is due to the presence of a metal core used to strengthen the magnitude of the induced magnetic field, but not necessarily the magnetic core is used. The presence of moving parts may lead to component wear and increase of the susceptibility to failure, which is not the case of the coils, because they are solid and potentially more robust.

The ADCS testbed designed and developed in the laboratory consists of an air bearing table, allowing it to move with low friction. The table has a limitation on the roll and pitch angles of $\pm 45^o$, which does not impose problems for the tests that are intended to be conducted using it.[5] It is instrumented with an Inertial Measurement Unit (IMU) of 9 Degrees of Freedom (DoF).[5] The IMU used is composed of three types of triaxial sensors: magnetometer, accelerometer and gyroscope. In addition to the IMU, a microcontroller, XBee radio for wireless communication, motor drivers, step motors for translational mass movement in three non-redundant degrees of freedom and batteries are embedded on the platform.[5]

For the simulation of the magnetic field in orbital conditions, the testbed is positioned inside a Helmholtz cage formed by a set of six squared coils, two for each axis of the cage, used to generate a homogeneous magnetic field according to the applied electric current.[5] The magnetic field simulated by the cage developed in LAICA is obtained from the World Magnetic Model (WMM) in Matlab, the software also controls automatically the current applied to the coils of the cage.[5,6]

Currently the cage is able to simulate magnetic field variations in magnitude and direction with intensities of $\pm 1.5G$ on all three axes.[6] The uniformity of the magnetic field in the center of the cage has been verified and guarantees the performance of tests with a magnetic actuator for the volume occupied by the table.[6]

DESIGN OF THE ACTUATOR

In order to develop the triaxial system, three electromagnetic coils were designed. Each coil shall generate an effective magnetic field oriented to the body axis of the spacecraft xyz.

Notions of Electromagnetism

The working principle of the coil as a magnetic actuator comes from the fact that the current carried through its windings induces a magnetic field $\vec{\beta}$, which makes it to behave as a dipole, originating a magnetic moment $\vec{m}$. The sense of the current passing through the windings of the coil defines the sense of induced magnetic field $\vec{\beta}$, given by the right-hand rule. The relation between

$\vec{m}$ and the torque $\vec{\tau}$ is given by Eq. (1), where $\vec{B}$ is the external magnetic field in which the dipole is located.[7]

$$\vec{\tau} = \vec{m} \times \vec{B} \tag{1}$$

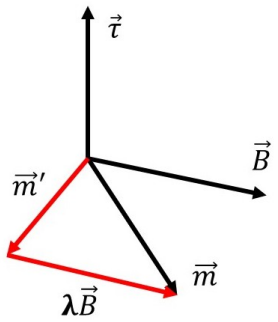

Figure 1. Analysis of the vectors $\vec{\tau}$, $\vec{m}$ and $\vec{B}$

From Eq. (1) it is clear that $\vec{m}$ must be increased in order to receive higher values of torque, since $\vec{B}$ depends on the orbit's height, and higher orbits presents lower intensities of geomagnetic field. If the equation is solved for $\vec{m}$, an interesting relation to determine the ideal magnetic moment for achieving a specific torque is found.[8] When conducting the resolution using the graphical representation in Figure 1, a general solution to the problem is given by Eq. (2), where $\lambda \in \Re$.[9,10]

$$\vec{m} = \frac{\vec{B} \times \vec{\tau}}{||\vec{B}||^2} + \lambda\vec{B} \tag{2}$$

A relation that allows to estimate $\vec{m}$ for a coil is given by Eq. (3) for N current loops.[11] In this equation I is the current through the loop, A is its area and $\hat{i}$ is the versor defined by the right-hand rule. The Figure 2 shows the an illustration of a cylindrical coil with its k layers.

$$\vec{m} = NIA\hat{i} \tag{3}$$

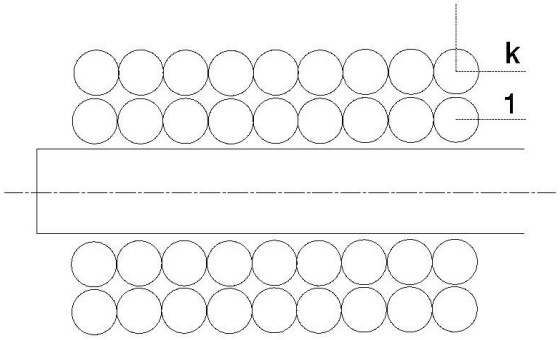

Figure 2. Representation of a cylindrical coil and its k layers

The presence of a magnetic core in electromagnetic coils may increase $\vec{\beta}$. The increase occurs when the material of the core has a positive magnetic susceptibility χ_m, which is the case for paramagnetic and ferromagnetic materials. The magnetic susceptibility measures the capacity of a given material to be magnetized by an external field. The effect of χ_m in the magnetic permeability μ is described by Eq. (4) and Eq. (5).[7]

$$\mu_r = (1 + \chi_m) \tag{4}$$

$$\mu = \mu_0 \mu_r \tag{5}$$

When a magnetic core of positive magnetic susceptibility is used in the coil, the magnetic field induced by the current magnetizes it, therefore the effect of the core's magnetization must be taken into account for the estimation of $\vec{m}$. The magnetization of a material $\vec{M}$ is the vector sum of all magnetic moments in a small portion of its volume divided by the volume, as seen in Eq. (6).[7]

$$\vec{M} = \lim_{\Delta v \to 0} \frac{1}{\Delta v} \sum_i \vec{m_i} \tag{6}$$

If the material is isotropic and linear Eq. (7) can be applied, where $\vec{H}$ is the field intensity.[7] If a linear relation exists between $\vec{M}$ and $\vec{H}$, then Eq. (8) can be considered.[7]

$$\vec{M} = \chi_m \vec{H} \tag{7}$$

$$\vec{\beta} = \mu \vec{H} = \mu_0 (\vec{H} + \vec{M}) \tag{8}$$

The Eq. (9) describes the magnetic moment for a solenoid with a core rod.[12] In this equation V_c is the volume of the core and $\vec{M}$ is its magnetization.

$$\vec{m} = NIA + V_c \vec{M} \tag{9}$$

System Requirements

The first step on the design of the electromagnetic coils was to define the requisites of dimension, mass and electrical power of the actuator system. In order to develop a modular dispositive compatible with CubeSats, the three coils shall be mounted on a Printed Circuit Board (PCB) with the form factor (length and width) in the PC/104 standard.

The electrical requirement that was imposed relates to the rated power at which the coils should operate. In order to determine this requirement, the power budget of the SERPENS nanosatellite was used as a reference. It was defined that the nominal power of each coil would be $300mW@5V$. It is emphasized that not necessarily the actuator will work intermittently, but in varying periods depending on the mission. The electrical power directly impacts electrical and dimensional characteristics of the actuator system, such as the resistance and minimum enameled copper conductor's diameter (gauge).

For the triaxial actuator being projected a limiting mass of 700g was adopted. This value was coherent in order to keep the mass of each coil less than $200g$. Due to this choice, at least $100g$ could be associated with the other components of the system such as electronic hardware, screws and structural materials.

The torque must clearly be maximized in order to increase the effectiveness of the actuator, and to do so, the magnitude of the magnetic moment $\vec{m}$ must be raised. For the development of the coils the torque was not specified, but the configuration that would lead to the highest values of $\vec{m}$ was searched. The requisites are summarized in Table 1.

Table 1. Design requirements of the system

Parameter	Description	Specification
$\vec{m}$	Magnetic moment of each coil	Maximization
P	Power per coil	$300mW$ @$5V$
M_b	Mass per coil	$< 200g$
M_t	Total mass of the system	$\leq 700g$
h_t	Height of the assembled system	$< 70mm$
C x L	Available surface (faces $\pm Z$ of the PC/104 board)	95.86 x $90.14mm$

Geometrical Configuration of the Actuator

In order to design the whole system two possible configurations for the actuator were taken into account. The first one considers three identical cylindrical coils with high magnetic permeability core mounted on the same face of a PCB, aligned with the X, Y and Z axes of the actuator.

This configuration was discarded in order to avoid increasing the complexity of the system due to the dimensions of the core. The main problem would be linked to the fact that one tip of the magnetic core on the Z axis would be fixed to the board, but to stabilize the other tip, a special structure would have to be developed to avoid stress concentration in a single region.

The referred stress concentration could cause problems due to the vibration of the system at the launch of the spacecraft, in the worst case damaging the board and other components. The vertical coil could be externally coupled from the actuator's board, but this configuration is not considered in this work because it was desired to construct a modular system integrated in a PCB.

The second configuration was chosen for the development (Figure 3), it considers two cylindrical coils with high magnetic permeability core on one face of the PCB (aligned with the Y and X axes) and a rectangular coil without core (vacuum of the space) taking advantage of the area in the opposite side.

Design of the Cylindrical Coil

In order to carry out the dimensioning of the cylindrical coil in compliance with the presented requirements, the illustration in longitudinal section of the winding shown in the Figure 4 was considered. In this figure, the lower part is in contact with the PCB's surface. Details regarding the observed dimensions in the figure were gathered in the Table 2.

The thickness t was defined as Eq. (10). The dimension h_1 was adopted to be $30mm$, $h_2 = 4mm$ and $L_s = 8mm$, these values are in accordance with the dimensional requisite. As higher is h_1 more layers of windings can be applied to the coil, then bigger is t.

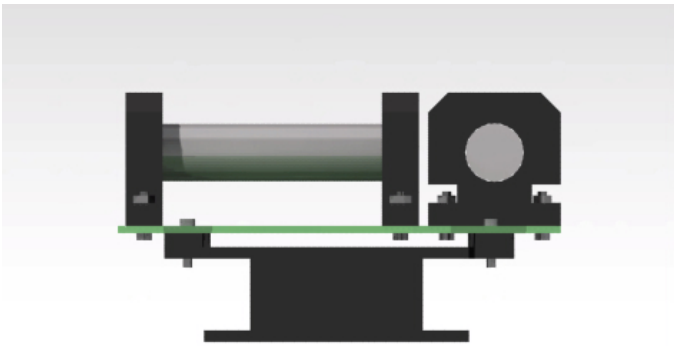

Figure 3. Illustration of the chosen configuration for the actuator

Table 2. Dimensional parameters of the cylindrical coil

Parameter	Description
L_c	Length of the core
L_b	Length of the winding
L_s	Support thickness
ϕ_c	Core diameter
h_1	Maximum height of the coil
h_2	Distance between the winding and the PCB
h_3	Thickness of the brace
h_4	Height of the support
t	Thickness of the layers of windings

$$t = k\phi_{\text{conductor}} \tag{10}$$

From geometrical analysis of the coil's representation on Figure 4, the relation between t, h_1, h_2 and ϕ_c is extracted and given by Eq. (11). Again, from geometrical analysis of the figure, Eq. (12) and Eq. (13) could be extracted. In order to calculate the possible number of turns in the available region defined by L_b, the Eq. (14) was used.

$$t = \frac{h_1 - h_2 - \phi_c}{2} \tag{11}$$

$$h_4 = h_2 + h_3 + t + \phi_c \tag{12}$$

$$L_b = L_c - 2L_s \tag{13}$$

$$N_e = \frac{L_b}{\phi_{\text{conductor}}} \tag{14}$$

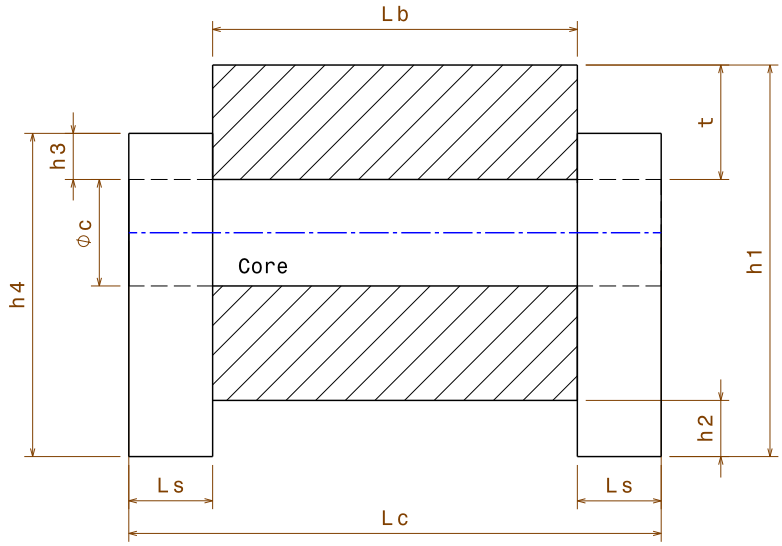

Figure 4. Illustration of the cylindrical coil with multiple layers and its dimensional parameters

The core material considered in this work was the EFI Alloy 79 due to its high maximum magnetic permeability, informed by the manufacturer to be $230,000$ (μ_r).[13] It's dimensions are $\phi_c = 12.7mm$ and $L_c = 64.5mm$. In order to find the configuration which would lead to the highest value of $\vec{m}$, it was created an algorithm in Matlab which have as inputs the system requirements and the following dimensions: L_c, L_s, ϕ_c, h_1, h_2, h_3, and h_4. It iterates as well the gauge of the enameled copper wires AWG 19 - 44.

The plot presented in Figure 5 was generated by the algorithm and indicates that the number of layers to reach the required power, corresponding to a resistance of 83.33Ω, approaches the maximum number of layers allowed when conductors of smaller diameters are used. This result was intuitive, because the resistance of the wire increases with the decrease of its diameter. Note that the conductors of higher AWG than 31 were automatically discarded by the algorithm because they were not adequate for the electrical current level of $0.06A$, value imposed by the power requisite of the system.

In this application the coil operates in Direct Current (DC), therefore its reactance X_L Eq. (15) was not considered and the solenoid was analyzed as being only resistive.[14] The Eq. (16) describes the relation between the current and the voltage for the inductor.[14] The impedance of the system is calculated as shown in Eq. (17), being equals to the resistance R for an inductor operating in DC.[14]

$$X_L = \omega L \tag{15}$$

$$V_L = L\frac{dI}{dt} \tag{16}$$

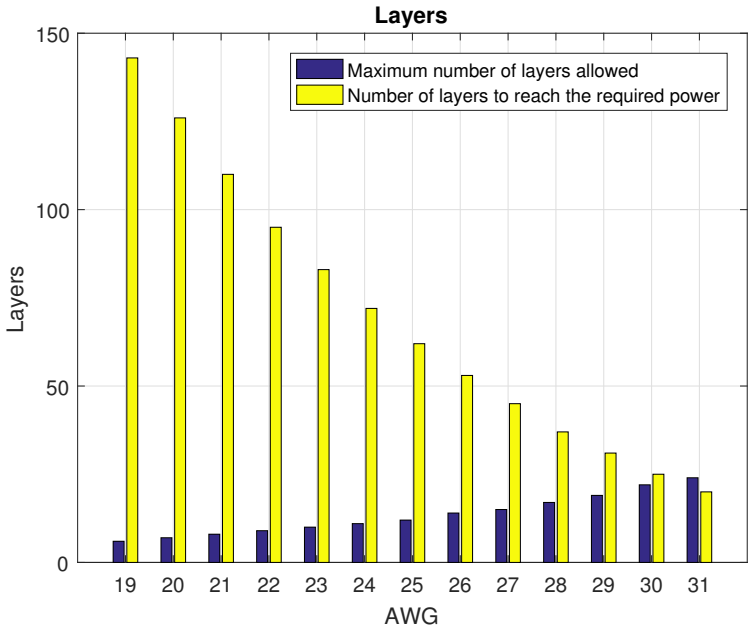

Figure 5. Comparison between the number of layers allowed and the number of layers to reach que required resistance for the cylindrical coil

$$Z = R + jX_L = \sqrt{R^2 + X_L^2} \angle \tan^{-1}\left(\frac{X_L}{R}\right) \tag{17}$$

The best configuration found by the algorithm for the cylindrical coil is shown in Table 3.

Table 3. Cylindrical coil designed

Parameter	Description	Value
$\|\|\vec{m}\|\|$	Magnetic moment	$0.358528 Am^2$
AWG	Gauge of the conductor	31
t	Thickness of the layers of windings	$5.48mm$
N_e	Number of turns	171
N_c	Number of layers	20
$L_{\text{conductor}}$	Length of conductor	$192.386485m$
$R_{\text{conductor}}$	Electrical resistance of the coil	84.842440Ω
R_{series}	Resistor to be associated in series	0Ω
$M_{\text{conductor}}$	Mass of conductor	$101.642087g$
M_c	Mass of the core	$70.359496g$
h_3	Thickness of the brace	$6.576mm$
h_4	Height of the support	$28.756000mm$

Design of the Rectangular Coil

The process of design of this coil was similar to what was conducted previously, but in this case no magnetic core was used. The illustration of the coil's structural support with its dimensional parameters is shown in Figure 6, they are summarized in Table 4.

The algorithm used to design the cylindrical coil was adapted in order to receive the parameters

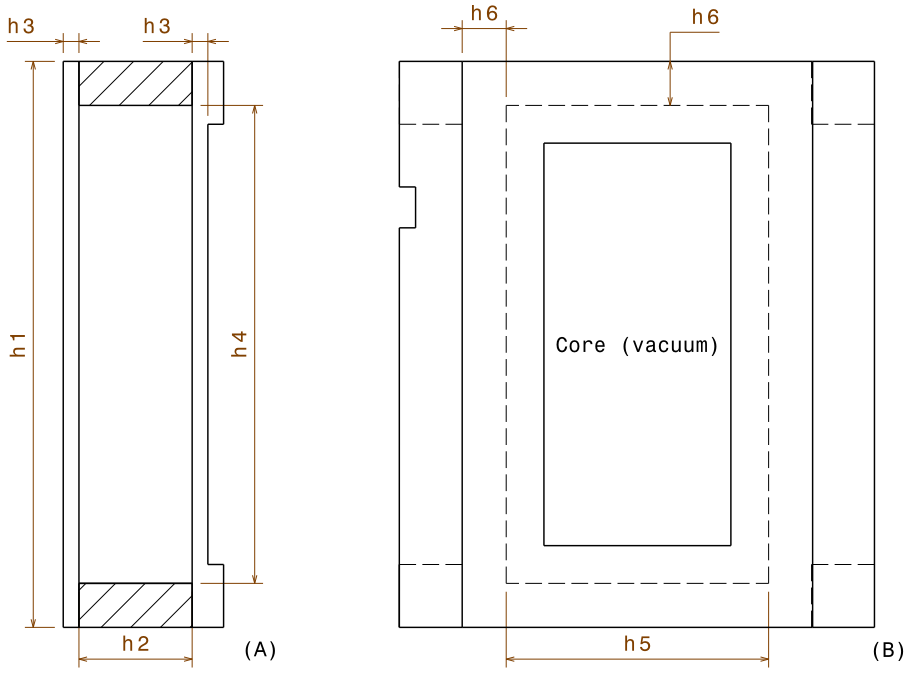

Figure 6. Illustration of the rectangular coil and its dimensional parameters

Table 4. Dimensional parameters of the rectangular coil

Parameter	Description	Value
h_1	Support height	$90.01mm$
h_2	Length of the winding	$18mm$
h_3	Thickness of the support	$2.5mm$
h_4	Length of the core	$76.01mm$
h_5	Width of the core	$41.73mm$
h_6	Thickness of the layers of conductor	$5mm$

which maximizes $\vec{m}$ for this case. The plot presented in Figure 7 shows the comparison of the maximum number of turns allowed and the number of turns to reach the power requisite.

Unlike the cylindrical coil, the structural support is part of the rectangular one, because the turns are winded directly on it. Therefore, the mass of the rectangular coil is the sum of the mass of its support and the mass of enameled copper conductors used. In order to determine the total mass of conductor that could be used in this coil, first the mass of the structural support was estimated Eq. (18).

$$M_{\text{conductor}} < 200 - M_{\text{support}} \tag{18}$$

The structural support was designed using the software CATIA V5R19, and to estimate its mass it was considered the usage of the material Windform XT 2.0 for its confection through a 3D printer. The analysis was conducted with this material because it is qualified for space applications in LEO.[15]

The manufacturer reports in his online catalog, that the material has a density of $1.097\frac{g}{cm^3}$ at

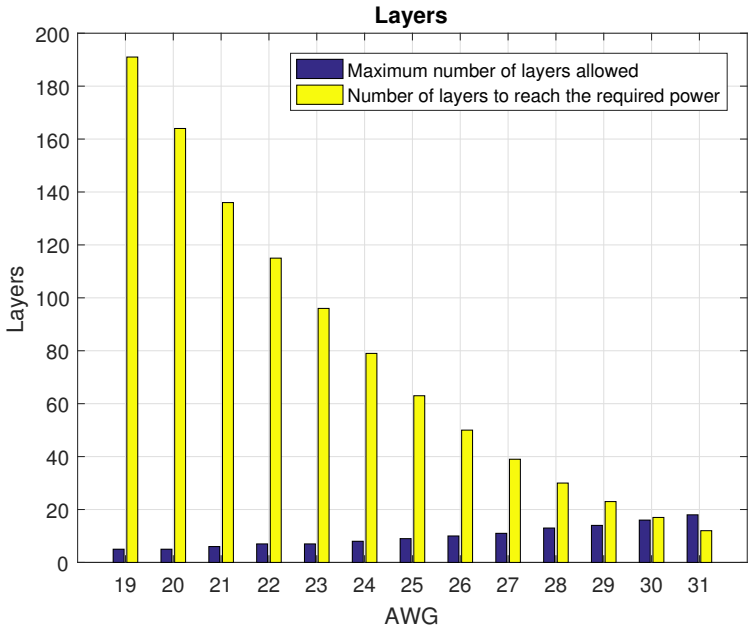

Figure 7. Comparison between the number of layers allowed and the number of layers to reach que required resistance for the rectangular coil

20^oC, and melting point at 179.30^oC.[16] Given the density value of the material, CATIA automatically provides the estimated part's mass, it was determined to be $M_{\text{support}} = 48g$. This information led to the conclusion that $M_{\text{conductor}} < 152g$.

The coil characteristics generated by the algorithm are shown in Table 5.

Table 5. Rectangular coil designed

Parameter	Description	Value
$\|\|\vec{m}\|\|$	Magnetic moment	$0.167236Am^2$
AWG	Gauge of the conductor	31
t	Thickness of the layers of windings	$3.288000mm$
N_e	Number of turns	65
N_c	Number of layers	12
$L_{\text{conductor}}$	Length of conductor	$193.078080m$
$R_{\text{conductor}}$	Electrical resistance of the coil	85.147433Ω
R_{series}	Resistor to be associated in series	0Ω
$M_{\text{conductor}}$	Mass of conductor	$102.007473g$

Design of the PCB

The electric circuit chosen to control the activation and deactivation of the coils is based on the H bridge principle, which allows the control of inductive loads, such as a DC motor or coils. In the case of motors it is possible, for example, to control the direction of rotation (clockwise or counterclockwise). This is due to the reversal of the direction of the current that results in the reversal of the direction of the magnetic field induced by the coils inside the motor. Thus it is evident that the application of the H bridge in the development of the electronic control interface of the triaxial actuator is convenient.

Based on the H bridge principle, the actuator driver can be implemented on a PCB using Texas Instruments L293D Integrated Circuit (IC), for example. Two units would be necessary, because each unit of this component allows the control of two loads. However, for the preliminary tests of the actuator the use of external controllers is sufficient. This integrated circuit allows the distribution of $600mA$ per channel for voltages in the range of 4.5 to 36V.

The printed circuit board with this component was designed, but it was decided that it would be developed in more advanced stages of research. The board has a double face, in $+Z$ the cylindrical coils would be placed and their terminals soldered to the board. In the opposite face, the rectangular coil would be located.

The board shall be powered by a 5V supply and connected to the onboard computer. The conductors coming from the onboard computer are used to transmit the logical signals to the actuator's integrated circuits, and the lines from the Electrical Power System (EPS) are used to provide the required power to the coils ($300mW@5V$).

DEVELOPMENT OF THE ACTUATOR

In this work the mission was to develop a prototype, not a flight model. Therefore, the structural supports of the coils were produced through a 3D printer using PLA.

Development of the Cylindrical Coils

A specific winding dispositive was developed for the production of the cylindrical coils through the 3D printing in PLA. The entire production process of the coils was manual, which made it time-consuming to achieve greater perfection in the uniformity of the windings. In average, the development of each coil has taken two days.

The first coil developed had good uniformity, but there was difficulty in keeping the turns aligned during the production process. Due to this fact, there was a moment in the production when it was no longer possible to be sure of the number of layers applied. This situation was clearly not ideal because there was no way to determine a criterion to stop winding.

As a manner to solve this issue it was decided to apply glue after finishing each k layer. The glue was applied to the wire turns, especially at the beginning and at the end of the layer. The Figure 8 illustrates in red the regions where the glue was applied at the beginning of the winding and in blue where the glue was applied between the layers.

The glue between the coil layers represented in blue in Figure 8 was not applied for all the wire turns, but only near the beginning and end of the winding. This was done in such manner for a double purpose, the first to prevent the increase of mass. The second is due to the diamagnetic property of the glue constituent material, so it is important to use only the minimum amount needed to prevent the decrease of the induced magnetic field strength. It is recalled that the diamagnetic material between the windings has the effect of weakening the magnetic field induced by the coil.

Due to the described usage of glue a higher quality coil was obtained as shown in Figure 9, presenting 10 winding layers. In this figure the designed structure for the production can also be seen, composed of two cylindrical rotors on each side of the core rod. It was ensured that in each layer all the turns were aligned and close to one another. The glue has allowed the development of a more robust device, where the windings will hardly be broken or will suffer relaxation. Therefore,

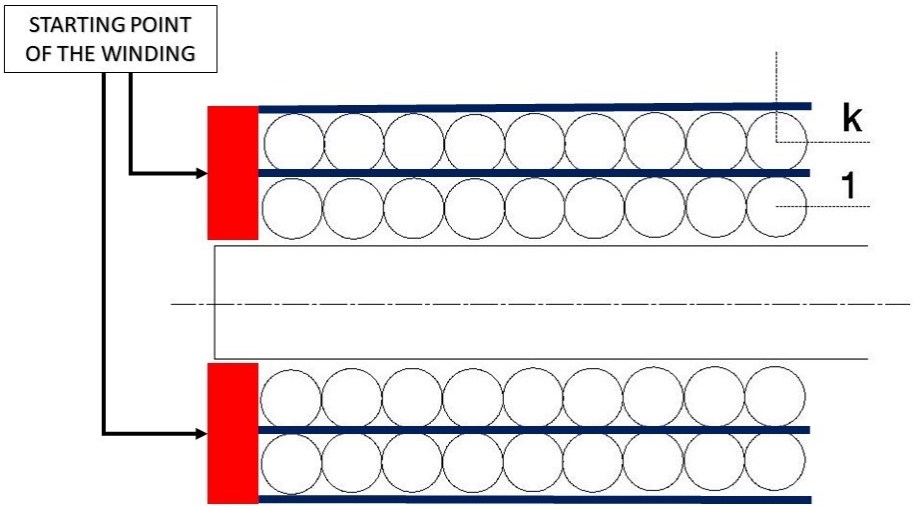

Figure 8. Regions where the glue was applied during the production of the cylindrical coils

this coil was considered adequate and its manufacturing method was applied for the development of the second electrical dispositive.

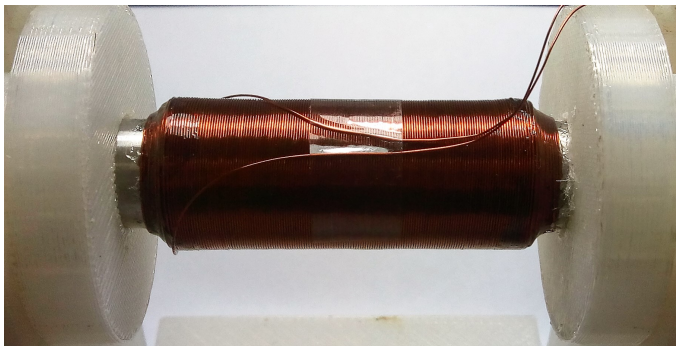

Figure 9. Cylindrical coil in development

The two produced coils are shown in the Figure 10. The number of layers applied was 10, less than that stipulated in the design (20 layers) due to the difficulty of the manual production. Thus it was decided to apply half of the value of layers, causing the expected magnetic moment to decrease. The new magnetic moment of the developed coils could be estimated by iterating the available data in another algorithm, the results are shown in the Table 6. In complement to the estimated characteristics, the measured properties were summarized in Table 7.

After both components be developed, the terminal wires of the two coils underwent a lacing process (cable harness), with the purpose not only of organization, but also to prevent damage and disassembling of the coils. By analysis of the information of Table 7 can be noted that the two coils developed have similar characteristics. The resistance to be associated in series is responsible for keeping the current passing through the solenoid lower than the limit sustained by their conductor wires, therefore it keeps the power close to the desired when the coil and the resistor are connected

Figure 10. Developed cylindrical coils

Table 6. Estimated characteristics of the developed cylindrical coils

Parameter	Description	Value
$\|\|\vec{m}\|\|$	Magnetic moment	0.17124
R	Resistance	35.930Ω
R_{series}	Resistor to be associated in series	47.403Ω

to the $5V$ power supply .

Development of the Rectangular Coil

For the development of the rectangular coil the windings were applied directly to the support in PLA. Unlike the development of the cylindrical coil, a winder was not developed for its production, also being made manually as it can be seen in the Figure 11.

During its production the wires were glued in the region of the four edges. The coil was developed with the 10 layers stipulated during the design phase, thus its estimated characteristics that were presented in the Table 5 are conserved for the constructed coil. Its measured characteristics are presented in Table 8.

Table 7. Measured properties of the developed cylindrical coils

Parameter	Description	Value
R_1	Resistance of the coil 1	34.5Ω
R_2	Resistance of the coil 2	37.1Ω
$R_{\text{series;1}}$	Resistor to be associated in series with the coil 1	$\geq 48.83\Omega$
$R_{\text{series;2}}$	Resistor to be associated in series with the coil 2	$\geq 46.23\Omega$
M_1	Mass of the coil 1 ($M_{\text{condutor}} + M_c$)	$100g$
M_2	Mass of the coil 2 ($M_{\text{condutor}} + M_c$)	$102g$

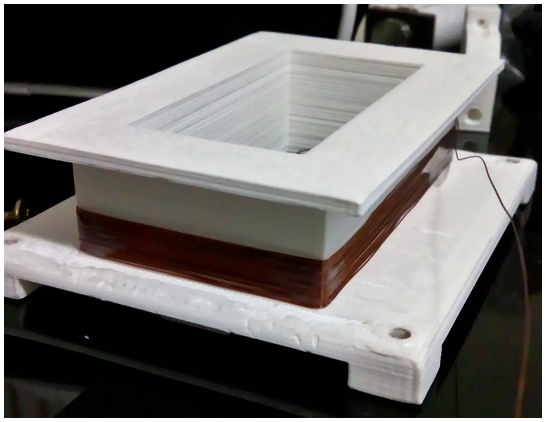

Figure 11. Development of the rectangular coil

Table 8. Measured properties of the rectangular coil

Parameter	Description	Value
R	Resistance of the coil	72.8Ω
R_{series}	Resistor to be associated in series with the coil	$\geq 10.53\Omega$
M	Mass of the coil	$118g$

Just like it was done for the cylindrical coils, the terminal wires passed through a harness process. When comparing the values of the Table 8 with the estimated data, it is noted that the values are not far from the expected.

INTEGRATION OF THE COMPONENTS

After the development of the coils it was possible to start the integration of the components in a PLA 3D printed board with the PC/104 form factor. This was done in order to provide an overall view of the system and to allow the conduction of the preliminary tests before the confection of a PCB with the embedded electronic components. The triaxial actuator integrated can be verified in Figure 12.

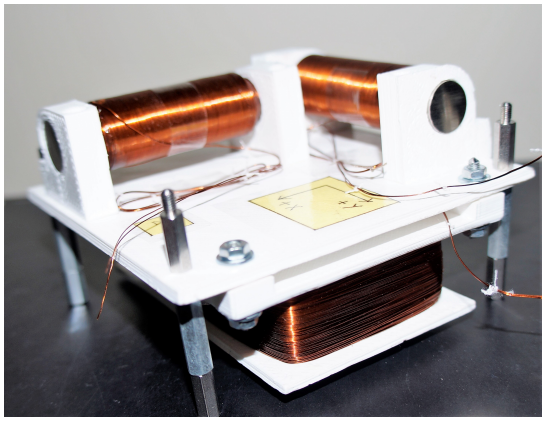

Figure 12. Magnetic actuator prototype integrated

MAGNETIC FIELD MEASUREMENT

The first preliminary test was conducted with the developed coils individually, through the measurement of their induced magnetic field using the 3 DoF magnetometer Honeywell HMR2300 through a Matlab interface. This test was conducted to prove that the coils were generating a magnetic field when the specified power was applied. In order to conduct this experiment, the axis of the coils where the greatest induced field was expected was aligned to the Z axis of the magnetometer. The coils were fed through the DC regulated power supply Minipa MPL-3303.

The values measured are summarized in Table 9. As it can be seen, the rectangular coil developed generates a stronger field than the others. This may have happened because the cylindrical coils were developed with less layers than they were originally designed. This fact results in a decrease of the field generated by them, and consequently decrease of their magnetic moment $\vec{m}$, but all the developed coils are fully functional.

Table 9. Measured magnetic field in μT

Coil	$\|\|\vec{\beta_x}\|\|$	$\|\|\vec{\beta_y}\|\|$	$\|\|\vec{\beta_z}\|\|$
Cylindrical coil 1	-26.69	20.24	103.2
Cylindrical coil 2	-15.15	-1.36	140.8
Rectangular coil	-211.3	-74.85	156.5

If the cylindrical coils were developed with the number of layers determined in the design, it would be expected that their generated magnetic field would be bigger than for the rectangular coil. All the values registered at the Z component are higher than the magnitude of Earth's geomagnetic field, which measures $50\mu T$ in average.[17]

CONCLUSION

The coils that integrates the triaxial magnetic actuator were developed and the measurement of their magnetic field was conducted, where it was possible to verify that the magnetic field is being induced by the current at the power specified during the definition of the system requirements. All the requisites were fulfilled, but in the case of the cylindrical coils, their development was conducted using an amount of layers smaller than stablished on the design due to the difficulty of a manual production.

As next steps of the research can be pointed the development of the PCB with the embedded electronics and conduction of the actuator function tests through the laboratory testbed. These tests may include the developed actuator integrated with an onboard computer such as ABACUS, or inside a nanosatellite.

ACKNOWLEDGMENTS

The authors thank the Brazilian National Council for Scientific and Technological Development (CNPq) for supporting this work through the grant Universal $421993/2016-2$. The authors thank as well the Foundation for Research Support of the Federal District (FAPDF), research grant $0193-000.216/2014$ (Edital 05/2013).

REFERENCES

[1] NASA, "What are SmallSats and CubeSats?," https://www.nasa.gov/content/what-are-smallsats-and-cubesats. [Online; accessed 25-November-2017].

[2] C. Gurgel, "The SERPENS program," http://www.asi.it/sites/default/files/attach/pagina/05_gurgel_-_aeb.pdf, 2016. [Online; accessed 25-November-2017].

[3] S. Battistini, C. Cappelletti, and F. Graziani, "An attitude determination and control system for a nanosatellite alternative launch platform," Guadalajara, Mexico, International Astronautical Congress (IAC), 2016, pp. 1–3.

[4] U. Kvell, M. Puusepp, F. Kaminski, J.-E. Past, K. Palmer, T.-A. Grönland, and M. Noorma, "Nanosatellite orbit control using MEMS cold gas thrusters," Estonian Academy of Sciences, 2014, pp. 279–284.

[5] R. C. da Silva, U. A. Rodrigues, R. A. Borges, M. Sampaio, P. Beghelli, S. G. P. d. Costa, B. T. Popov, S. Battistini, and C. Cappelletti, "A testbed for attitude determination and control of spacecrafts," Florianpolis-SC, Brazil, II Latin American IAA CubeSat Workshop, 2016, pp. 2–13.

[6] L. C. v. d. Ploeg, "Desenvolvimento de sistema para simulação do campo magnético terrestre em órbitas baixas," 2017. Trabalho de Graduação em Engenharia de Controle e Automação, Publicação FT.TG-nº010/2017, Faculdade de Tecnologia, Universidade de Brasília, Brasília, DF.

[7] J. R. Reitz, F. J. Milford, and R. W. Christy, *Fundamentos da Teoria Eletromagnética*. Campus, 3 ed., 1982. pp. 166-244.

[8] G. F. d. Oliveira, P. H. D. Nehme, and C. Cappelletti, "Analysis and Simulation of Attitude Determination and Control for the SERPENS Nanosatellite," International Academy of Astronautics (IAA), 2014, p. 14.

[9] M. Loulidi, "Mecanique du Solide," http://www.fsr.ac.ma/cours/physique/Loulidi/cours0809.pdf, 2008. [Online; accessed 25-November-2017].

[10] A. Kassoul, "Rappels mathématiques (éléments de calcul vectoriel)," http://www.univ-chlef.dz/fgca/images/chapitre_1__rappels_mathmatiques_lments_de_calcu%20l_vectoriel.pdf. [Online; accessed 25-November-2017].

[11] D. Acosta, "Magnetic Dipoles," http://www.phys.ufl.edu/~acosta/phy2061/lectures/MagneticDipoles.pdf. [Online; accessed 25-November-2017].

[12] N. Bellini, "Magnetic Actuators for Nanosatellite Attitude Control," Università di Bologna, Tesi di Laurea, 2013/2014. pp. 67-126.

[13] "EFI Alloy 79," http://www.edfagan.com/litPDF/Alloy79_4-29-09F.pdf. [Online; accessed 25-November-2017].

[14] J. A. Edminister, *Circuitos elétricos*. São Paulo: Pearson Education do Brasil Ltda., 1991. pp. 6-490.

[15] T. Clements, G. Moore, A. Clements, S. Davis, J. White, D. Wilt, W. Holemans, J. Rexroat, N. Fite, D. K. PhD, B. M. PhD, and J. L. PhD, "3D Printed Parts for CubeSats; Experiences from KySat-2 and PrintSat using Windform XT 2.0," International Academy of Astronautics (IAA), p. 9.

[16] "Windform XT 2.0," http://www.windform.com/PDF/SCHEDA_WF_XT_2_0_ENG.pdf. [Online; accessed 25-November-2017].

[17] "Earth's Magnetic Field," https://sciencedemonstrations.fas.harvard.edu/presentations/earths-magnetic-field. [Online; accessed 25-November-2017].